Optically detected magnetic resonance via the magnetic circular dichroism of absorption of cerium impurities in bulk paramagnetic terbium gallium garnet

1997 J. Phys.: Condens. Matter 9 9065

(http://iopscience.iop.org/0953-8984/9/42/020)

J. Phys.: Condens. Matter **9** (1997) 9065–9082. Printed in the UK PII: S0953-8984(97)83797-6

Optically detected magnetic resonance via the magnetic circular dichroism of absorption of cerium impurities in bulk paramagnetic terbium gallium garnet

H-J Reyher†, B Faust†, B Sugg†, R Rupp† and L Ackermann‡

† Fachbereich Physik, Universität Osnabrück, D-49069 Osnabrück, Germany

‡ Forschungsinstitut für Mineralische und Metallische Werkstoffe, D-55743 Idar-Oberstein, Germany

Received 29 April 1997

Abstract. The paramagnetic resonance of dilute Ce^{3+} ions in the bulk paramagnetic host $Tb_3Ga_5O_{12}$ is separated from the host response by means of optically detected magnetic resonance (ODMR) using the magnetic circular dichroism (MCD) of the absorption. This result shows that it is possible in principle to extend by means of the ODMR of the absorption the regime of paramagnetic resonance detection of impurity ions to magnetic hosts, which strongly interact with the microwave field and, hence, make the impurity signals unobservable by means of conventional EPR. The observed ODMR signals are attributed to Tb^{3+} and Ce^{3+} ions by correlation with the optical bands of these species. By means of ODMR via the Faraday effect it is shown that this effect is due to transitions between Tb levels. The identification of the observed magnetic resonance structures is confirmed by calculations based on known information on Tb^{3+} and Ce^{3+} in diamagnetic hosts. The role of molecular fields is discussed.

1. Introduction

Terbium gallium garnet $Tb_3Ga_5O_{12}$, henceforth abbreviated as TGG, is an interesting representative of the family of rare-earth garnets without iron. These garnets have been widely investigated because of their interesting magnetic and optical properties [1]. TGG is also of technological interest, since it shows, at the same time, a relatively large Verdet constant and a wide spectral transparency range, which makes TGG a useful substance for Faraday rotator devices, in particular for optical isolators [1].

Recently a photo-refractive effect (PRE) has been found in TGG and was attributed to photo-induced changes δn of the refractive index, which are connected by the Kramers–Kronig relations to a photochromic absorption band resulting from an impurity ion [2]. To our knowledge this is the first direct observation of a PRE, which results from the contributions to δn of an impurity ion alone, instead of δn originating from the host material, as is the usual case [3]. In this paper we shall identify the impurity ion responsible for the PRE in the TGG sample of reference [2] as Ce^{3+} by using the method of optically detected magnetic resonance (ODMR) via the magnetic circular dichroism (MCD) of the absorption. As will be described briefly in the following section, this technique allows one to correlate information gained from magnetic resonance with that obtained by absorption spectroscopy. This is usually done by starting from the known EPR properties of the impurity ion in question and by then transferring via ODMR this 'EPR fingerprint' to the optical absorption bands. If the host is paramagnetic, however, there may be a strong non-resonant response

0953-8984/97/429065+18$19.50

from the bulk magnetism, which covers all possible signals from any impurities and thus makes conventional EPR spectroscopy impracticable. Experiments using a Bruker EPR spectrometer at X-band frequencies showed that this is the case for TGG. In this report we will demonstrate that MCD-ODMR, in contrast to EPR, allows one to observe magnetic resonance signals from both the bulk (Tb^{3+}) and from impurity ions (Ce^{3+} in TGG). It is true that these signals are very broad and uncharacteristic, but the correlation with the optical properties, provided by the method itself, allows a consistent interpretation of optical bands and ODMR signals. Also the comparison with data for these ions in diamagnetic garnets, YAG for example, confirms the identification of the ODMR signals. As a result it is shown here that the field accessible to paramagnetic resonance spectroscopy may in principle be extended to ions in strongly interacting magnetic hosts. This may be of particular interest for magneto-optical materials.

There exist cases where conventional EPR of impurities in similar paramagnetic garnets, like $Eu_3Ga_5O_{12}$ or $Tm_3Ga_5O_{12}$, can be observed unaffected by 'background signals' from the host material and with signal widths of the same size as in diamagnetic hosts, the resonances being shifted only slightly by the interaction with the matrix (see [4] and later work cited in [1]). The strikingly different situation for TGG is related to a different spacing of the electronic levels of the rare-earth ions. All of these ions—Tb^{3+}, Eu^{3+}, Tm^{3+}, and others—have an even number of electrons in the 4f shell, and this configuration leads to free-ion levels with integer quantum numbers for the total angular momentum $\boldsymbol{J}$. Since the rare-earth site in garnets shows symmetry D_2, all of these levels split to singlet crystal-field levels. These singlets are non-magnetic because of time-reversal symmetry, but in an external field a magnetic moment is induced by the Zeeman interaction mixing the singlets (Van Vleck paramagnetism). If Δ indicates the energy difference between the two lowest singlets, only the lowest singlet is occupied for $k_BT \ll \Delta$, leading to temperature-independent magnetic susceptibilities χ. From the data collected in [1], one may see that χ for TGG depends strongly on T down to $\approx$2 K, in contrast with the results for Eu–Ga/Al and Tm–Ga/Al garnets. This indicates that Δ is very small for TGG in contrast with the other crystals. In fact, our ODMR results for Tb^{3+} show that Δ is between 2 and 3 K, which has to be compared with 100 K for Tm^{3+} [4] or 500 K for Eu^{3+} [5]. Even at liquid helium temperatures one has $k_BT \approx \Delta$ for TGG in contrast with $k_BT \ll \Delta$ for the other garnets. As discussed in [4], the relaxational transitions to the first excited singlet are suppressed under the condition $k_BT \ll \Delta$ and the interaction of the induced magnetic moment of the host rare-earth ion with the spin of the impurity becomes time independent. Consequently, the EPR line of the impurity ion is not broadened in comparison with that of diamagnetic hosts, and EPR signals from the host are absent since the usual microwave quanta energies are of the order of a few degrees Kelvin. Obviously the opposite is the case for TGG, which makes this crystal inaccessible to EPR investigations. Finally, the small value of Δ also explains the strength of the Faraday effect in TGG, which is connected with Tb^{3+} levels, as we shall show in this work, too.

2. Experimental procedure

The TGG crystals investigated were grown by the Czochralski technique at Idar-Oberstein†, the samples being described in table 1. Ca was added to the melt to improve the crystal growth, and Ce to avoid by means of charge compensation the generation of colour centres

† Forschungsinstitut für Mineralische und Metallische Werkstoffe, Idar-Oberstein, Germany.

Table 1. The properties of the TGG samples investigated. The numbers in the second column indicate the doping of the melt in weight ppm. *d* is the diameter, and *l* the length in mm of the cylindrically shaped samples. The Ce and Ca surpluses of S1 and S2 were unintentional [6].

	Doping			Size		
Sample	Ca	Ce	Colour	*d*	*l*	Remarks
S1	25	25	Yellowish	5	7.8	Ce surplus
S2	60	60	Brownish	4.6	5	Ca surplus
S3a/b	Undoped		Colourless	5	2/8	
S4	25	65	Yellowish	5	4	

caused by Ca doping [7]. No attempt was made to estimate the impurity ion concentration in the crystals. All of the samples were cylinder shaped with their axes parallel to [111], and polished ends.

The MCD of the absorption, the ODMR via the MCD of the absorption, and the tagged MCD were measured using a conventionally designed system consisting of an Oxford 3 T magnet cryostat, 35 and 70 GHz microwave equipment, and an optical set-up suitable for polarization spectroscopy (a xenon arc lamp, monochromator, elasto-optical modulator, and photomultiplier) [8, 9]. A special aspect of our set-up consists in the fact that we do not use microwave cavities, but mount the samples at the end of a 35 GHz waveguide. The same waveguide is used for 70 GHz with acceptable losses. The sign of the MCD has been checked as described in [10].

For the crystals investigated, we encounter a special problem for MCD measurements, because the strong Faraday rotation in TGG often leads to effects of interference with the MCD signals. From a general analysis of the modulation technique in polarization spectroscopy [11], one may see that, for non-zero linear dichroism or birefringence, the MCD signals are influenced in a complicated way by the Faraday rotation, if the usual lock-in detection on the fundamental frequency of the modulation is applied. Linear anisotropic reflection from the lenses and the crystal surface arises when the crystal is tilted with respect to the optical axis. For small tilting angles, due to misalignment this usually leads only to a very weak 'effective' linear dichroism, which scarcely disturbs the MCD measurements for most samples. In Faraday-active TGG, however, it is sufficient to produce a substantial and almost unavoidable effect of interference of the MCD and Faraday rotation. This cross-talk effect was present whenever the set-up showed linear anisotropy, and could always be reduced by careful alignment of the optical components perpendicular to the optical axis. The effect will be demonstrated in section 3.3.

The Faraday effect has been measured by replacing the acousto-optical modulator of the MCD set-up by a rotating linear polarizer and inserting a static linear polarizer into the optical path behind the crystal. It is easily seen that the Faraday rotation angle is proportional to the phase of the modulated signal, which was recorded using a two-phase lock-in amplifier.

A further experimental peculiarity arises from very sharp MCD features at the Tb^{3+} absorption lines. Since our set-up comprises a monochromator with a focal length of 20 cm, these sharp MCD lines can only partly be resolved even with the smallest slit widths. Even minor changes of the geometry of the optical system lead to different spectral behaviour of the MCD around the rare-earth lines. However, the overall structure was similar from run to run, and we therefore omitted the very careful adjustment which was needed to reproduce exactly the shape of the sharp MCD spectra from terbium.

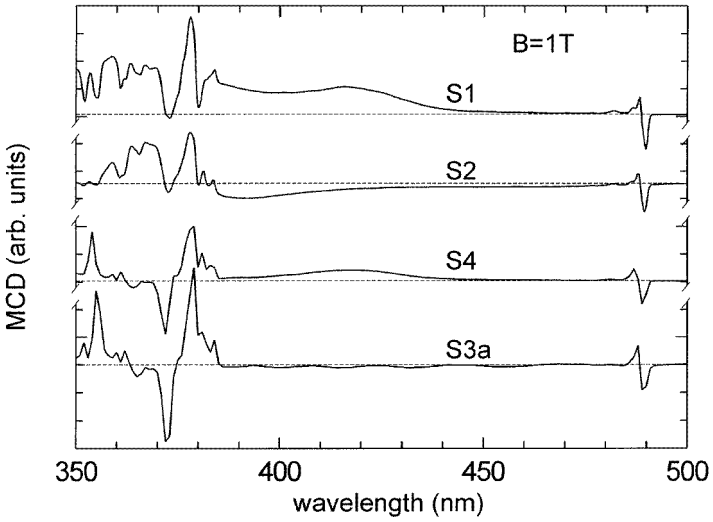

Figure 1. MCD spectra of the TGG samples investigated. The spectral resolution was slightly different from trace to trace. This partly explains why the region of the Tb^{3+} lines at 488 and below 385 nm shows different features (see the text).

3. Experimental results and discussion

3.1. MCD

The MCD spectra at 1 T of samples S1, S2, S3a, and S4 are shown in figure 1. One may distinguish broad and narrow features. The latter ones are similar for all probes and are easily attributed to Tb^{3+}, since the lines are characteristic for this rare-earth ion [12, 13]. At room temperature, the lines below 385 nm are covered by the band edge and are therefore not resolved in the absorption spectrum shown for sample S1 in [2].

Broad bands between the Tb lines are only seen for the doped samples. A positive MCD band is centred at around 420 nm in the spectra of S1 and S4. This band is well separated from the Tb lines and is attributed to Ce^{3+} with the help of the ODMR results presented below. The attribution to Ce^{3+} is further supported by the fact that a similar band at 450 nm is well known in $Y_3Al_5O_{12}$:Ce, where it was assigned to a 4f–5d transition of Ce^{3+} [14, 15]. The positive MCD band of Ce^{3+} at 420 nm (hereafter called 'Ce band') is identical with the photochromic absorption band found by Sugg, which has been connected with the existence of the photo-refractive effect in TGG:Ce:Ca [2], as mentioned in the introduction. We therefore identify Ce^{3+} ions as the impurity ions which are, in connection with other—unidentified—charge-carrier traps, responsible for the PRE in these TGG crystals. The illumination of the crystal with the weak probe light did not lead to observable photochromic effects in the measurements presented here.

Two further broad MCD features are seen in figure 1. A positive band, with the high-energy lines of Tb superimposed on it, is found at around 370 nm for samples S1 and S2, and the latter sample shows in addition a negative band at around 390 nm. These two MCD bands could not be attributed to a specific ion by means of ODMR, since only magnetic resonance signals of Tb ions were seen there (section 3.2). It is straightforward to connect the negative band with the brownish colour of S2, which has been attributed to a Ca surplus [6]. However, the relevant colour centre cannot be identified here, since, as mentioned, no

corresponding ODMR signals could be observed.

In the region between the Tb lines of the MCD spectra of S3a, we observe the signal to wave around the zero line. These wiggles arise from the interference between the Faraday rotation and MCD, as mentioned in the previous section. They reflect the dependence of the Verdet constant on wavelength [1]. In figure 1 this effect is only seen for S3a, since this sample had slightly non-parallel end surfaces. It was thus impossible to avoid the cross-talk effect here.

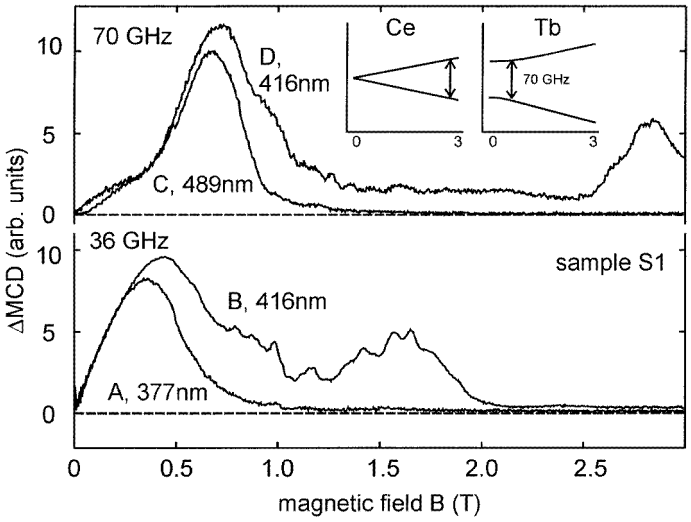

Figure 2. ODMR spectra of sample S1. The change of the MCD caused by microwave transitions is plotted as a function of the magnetic field. The positive sign corresponds to a decrease of |MCD|. For both frequencies, two wavelengths characteristic for Tb and Ce MCD have been chosen. The wiggles to be seen above 0.5 T result from an artefact (see the text). The inset depicts the splitting of the two lowest levels of Ce^{3+} and Tb^{3+} according to calculations presented in appendix A.

3.2. ODMR

In figure 2 ODMR signals at 35 and 70 GHz are shown by plotting, as a function of B, the difference ΔMCD between the MCD signals with the microwave power off and on. The positive sign corresponds to a decrease of |MCD| when resonance occurs, which represents the usual sign of ODMR signals arising from simple spin systems such as, e.g., spin doublets. All of the curves have been recorded using sample S1. For each frequency, 36 and 70 GHz, a trace has been taken, one with the MCD monitor on a Tb line at 377 or 489 nm (curves A and C) and one using the MCD at 416 nm, near the centre of the Ce band (curves B and D). Other wavelengths, characteristic for each ion, were chosen and showed the same ODMR signals. In order to avoid two-quanta transitions (see appendix B), the spectra for 36 GHz were recorded at reduced microwave power. The pairs of spectra A/B and C/D have been scaled appropriately in order to obtain approximately the same dependence for fields below 0.3 T, since these are the only regions in which the spectral shape is similar for the pairs.

The ODMR signals are very unusual. In comparison with ordinary paramagnetic resonance experiments, the scale on the abscissa is large, and the signals start from zero

field and are extremely broad. Also the flat region of spectrum D between 1.4 T and 2.5 T as well as the long tail above 2 T in spectrum B are surprising. We shall comment on these peculiar details in appendix B. In addition, the wiggles visible on the ODMR spectra (see section 3.3) will be ignored temporarily. Instead we focus on the main features of the ODMR spectra and will give the most plausible assignments of the observed magnetic resonances to the relevant ions.

First, the high-field humps at 2.8 and 1.7 T for 70 and 35 GHz, respectively, are attributed to Ce^{3+}. These structures are seen only via the broad positive MCD band at 420 nm and occur only for samples S1 and S4, exhibiting a Ce surplus with respect to the Ca doping. This is consistent with our above-mentioned assignment of this band to an optical transition of Ce^{3+} and with the assumption of charge compensation among Ce^{4+} and Ca^{2+} as the de-colouring effect for equally doped crystals, as mentioned in section 2. A Ce surplus may then lead to the incorporation of Ce ions in the 'ordinary' charge state (3+) of rare-earth ions in garnets. ODMR transitions at the observed positions are also to be expected by comparison with EPR data for Ce^{3+} in diamagnetic garnets, as will be discussed in appendix A. The results obtained there are displayed in the schematic Zeeman diagrams shown as insets in figure 2.

Second, the ODMR bands below $\approx$1 T are attributed to magnetic transitions of Tb^{3+}. Of course this assignment is supported by the fact that bands of similar shape are found, if the MCD of Tb (curves A and C, 377 and 489 nm) is used as a monitor for the ODMR. These low-field signals are also observed in the undoped sample S3 with similar strength and shape. In addition, we find equivalent resonances by means of ODMR detected via the Faraday rotation (see the following section), which is a typical bulk property and almost unaffected by dilute impurities like Ce. Finally, the results of crystal-field calculations (see appendix A) suggest low-field transitions for 70 GHz because of a large zero-field splitting, as sketched in the insets in figure 2.

We will explain in detail in appendix B, that the given assignment also agrees with a number of puzzling properties of the Tb-related ODMR signals: magnetic transitions are also observed for 36 GHz and the corresponding low-field ODMR signals peak at roughly half the field found for 70 GHz. At first glance, this seems to contradict the Zeeman diagram of Tb. The ODMR of Tb can be observed using the MCD of both Ce and Tb. Finally, there is a shift of the Tb-band maximum or an additional shoulder at higher magnetic fields when the MCD of Ce is the probe signal, especially in the case of the spectra for 36 GHz (compare spectra B with A and D with C in figure 2).

Assuming the given attribution to be exact, it is shown by figure 2 that magnetic resonance of both the host ions Tb and the impurities Ce may be observed by means of ODMR. It might then be surprising that the signals from Tb^{3+} have the same size as those from Ce^{3+}, although the latter ions are diluted by at least a factor of 10^{-5} with respect to Tb. Indeed, in conventional EPR the response to the host is so strong that the microwave bridge cannot be kept tuned for $B \neq 0$. The comparable sensitivity of ODMR for Tb and Ce results simply from the fact that the MCD, being the monitor signal for the ODMR, is of the same order of magnitude for these two ions, as one may see in figure 1. The ODMR lines are scaled by the strength of the MCD and not just by the spin density, as is the case in EPR.

3.3. Faraday rotation

Faraday rotation (FR) or magnetic circular birefringence (MCB) is connected with MCD by the Kramers–Kronig relations [16]. Consequently, if paramagnetic MCD is present,

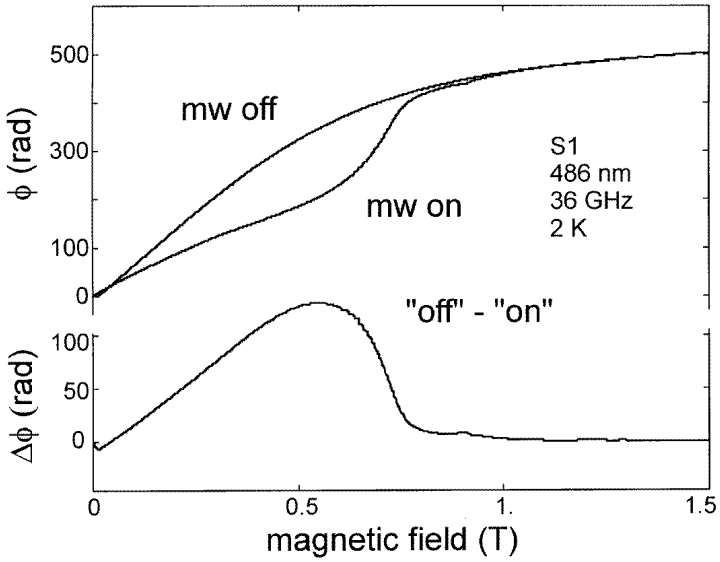

Figure 3. The ODMR of Tb^{3+} ions observed via the Faraday effect of sample S1. The upper curves shows the measured rotation angle Φ as a function of the magnetic field B with the microwave field off and on. The change of $\Phi(B)$ caused by microwave transitions is plotted below (36 GHz). Note that the rotation at 2 K is much stronger than that at room temperature due to the different population of the Tb levels.

paramagnetic FR may also be observed. There seems to be agreement that within regions of absorption, MCD is the experimentally preferred quantity, and FR outside [17]. In the case of TGG, the strong FR from the host will by far dominate over the contributions from dilute impurities, like Ce, even in a spectral region where this impurity shows an absorption band†. In view of the spectral dependence of the Verdet constant, showing a smooth decay starting at the band edge [1], one may assume that the transitions connected with MCB are located close to the band edge, where the f lines of Tb become numerous and where also the strong 5d transitions are to be expected [18]. One may therefore assume that transitions to Tb levels are responsible for the FR in TGG. The ODMR observed via FR should consequently show the Tb^{3+} resonances alone. The corresponding result is depicted in figure 3 for a monitor wavelength of 486 nm, but the same result has been found for other wavelengths including 420 nm. The resonance curve from figure 3 is similar‡ to the corresponding MCD-ODMR spectrum at 36 GHz (curve A in figure 2). This confirms our assignment of the low-field ODMR transitions to Tb^{3+} ions. Conversely, the above-assumed attribution of the FR effect to Tb transitions is confirmed by consistency. It should further be noted that saturation of the Faraday rotation starts at 1.5 T. This is consistent with the calculations presented in appendix A, where we find that the magnetic properties of the terbium ground state start to saturate at this field (see figure A1 later).

Having presented the main results on the MCD-ODMR and FR, we may now discuss the cross-talk effect (CTE) between the FR and MCD, which leads to the wavy structure

† The contribution of the Ce band at 420 nm to the refraction index of the sample is very weak and could be detected by refined holographic methods only [2].

‡ The shift of the maximum of the FR-ODMR results from the enhanced microwave power used here (see appendix B).

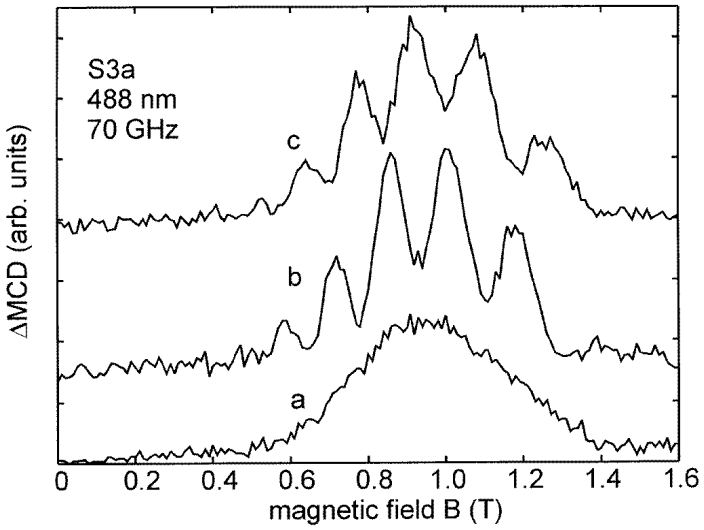

Figure 4. The effect of cross-talk between the MCD and FR on the 70 GHz ODMR of Tb for the disc-shaped sample S3a. In spectrum (a) the effect is absent, while in spectra (b) and (c) it is activated by inserting a horizontally and vertically tilted glass plate into the optical path (see the text).

of the ODMR signals, especially pronounced between 0.5 and 1.5 T in spectrum B of figure 2. It is important to identify this structure as an artefact, since a physical origin would clearly influence the interpretation of the spectra. As already mentioned in section 2, the CTE arises from the simultaneous presence of linear dichroism in a very complicated way [11]. It would require further detailed information to estimate, by use of the general formulae given in [11], the impact of the CTE on the ODMR signals as shown in figure 2. Therefore we investigated this effect empirically. Figure 4 shows the 70 GHz ODMR at reduced microwave power of Tb^{3+} of sample S3a, which is only 2 mm long. Compared to spectrum C in figure 2 the non-resonant tail at low fields (see appendix B) is weaker due to the reduced power and the peak is shifted to higher magnetic field because of the different demagnetization field (see appendix A). Curve (a) is obtained with optimally adjusted optical components, and curve (b)/(c) with a horizontally/vertically tilted glass plate in the optical path. The modulation of the MCD signal by the CTE has opposite phases in (b) and (c), since the effective LD, caused by the plate, changes sign when the orientation of the plate is altered. From the upper part of figure 3 one may obtain for sample S1 near 1 T a 'rotational power' $\mathrm{d}\phi/\mathrm{d}B$ of $\approx$160 rad T^{-1}. Correcting for different sample lengths yields $\mathrm{d}\phi/\mathrm{d}B \approx 40$ rad T^{-1} for S3a. By counting the full periods in figure 4, approximately the same number is obtained. This shows that the CTE leads to a superimposed lock-in signal exhibiting a phase, with respect to the modulation reference, proportional to ϕ. The reason for this apparently simple relation has not yet been understood. We have chosen a shorter sample and reduced microwave power here, because the CTE could only be demonstrated in such a clear way for relatively low values of $\mathrm{d}\phi/\mathrm{d}B$ and for small microwave-induced $\Delta\phi$. For higher values of $\mathrm{d}\phi/\mathrm{d}B$ the CTE is averaged out. Therefore it is not observed below $\approx$0.5 T. For higher values of $\Delta\phi$ (enhanced microwave power) the wiggles become irregular (see figure 2), the reason for this being unclear, too.

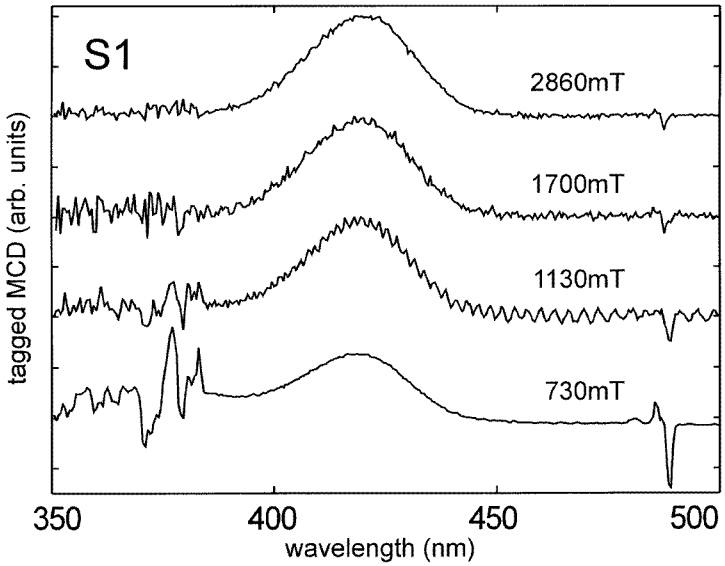

Figure 5. Tagged MCD spectra of sample S1 for several magnetic fields and for 70 GHz. The spectra have been scaled differently. The enhanced noise below 385 nm for some spectra results from the changed sensitivity.

3.4. Tagged MCD

At some fixed values of the magnetic field B, the difference between the MCD signal with microwaves 'off' and 'on' is recorded as a function of wavelength. The resulting spectrum is called tagged MCD, since it represents the MCD of the paramagnetic defect, which is magnetically resonant at the selected field. The tagged MCD spectra shown in figure 5 were taken at 70 GHz, since the resonances of Tb and Ce are well separated for this frequency compared to 36 GHz (see figure 2). In principal, however, similar results are obtained for 36 GHz. We shall show now that these spectra may be explained consistently using the given assignment of MCD and ODMR bands to the species Ce^{3+} and Tb^{3+}. The tagged MCD spectra of the two species are separated, if the corresponding magnetic resonance transitions are disconnected. This is shown by the uppermost spectrum in figure 5, which was recorded at $B = 2.86$ T, a field corresponding to the resonance position of Ce^{3+} (figure 2, spectrum D). The MCD band of Ce is isolated, the Tb lines being strongly suppressed. On the other hand, however, it is not possible to isolate the MCD of the paramagnetic host ions Tb^{3+}. This is shown by the tagged MCD spectrum at 0.73 T, where the ODMR of Tb^{3+} is located. The Ce band is still visible there. Of course this finding is consistent with the ODMR spectrum D in figure 2, observed via the Ce MCD at 416 nm. There, the Tb resonance is *not* absent, as is found usually for two uncoupled species in diamagnetic hosts. One may say that the tagged MCD method is only semi-selective here. As explained in appendix B, this feature results from the magnetic coupling between Tb and Ce ions.

We discuss now the tagged MCD spectra at 1.7 and 1.13 T, where the Ce band is dominant but the Tb lines become visible. Both fields are within the flat background-like ODMR signal between the Tb and Ce resonances (figure 2, spectrum D). In appendix B we shall attribute this background signal to non-resonant heating of the spin system by the microwaves and argue that this effect is more efficiently detected via the MCD of Ce than

that of Tb. Consequently the background signal is stronger for spectrum D compared to C in figure 2 and, consistently, the tagged MCD spectra recorded in this region (1.13 and 1.7 T) exhibit an enhanced Ce band, if compared with the Tb lines.

4. Summary

The results presented have shown that ODMR of dilute impurity ions is feasible in principle also for magnetic host crystals, where resonance signals of these impurities are completely buried by the host response in conventional EPR. If the ODMR signals of the host and impurity are separated from each other, as is the case for TGG:Ce for 70 GHz, the tagged MCD method may then be applied to reveal the impurity-related optical bands. In this way the Ce band at 420 nm could be definitely identified in TGG. This band has been correlated with a novel photo-refractive effect in this material [2]†.

Severe problems have to be overcome in ODMR experiments of this type. First, the resonances are heavily broadened by the impurity–host interaction (unless some line narrowing effect is present). As we found in the present case, this broadening may cover smaller line splittings and hyperfine structure and the ODMR curves become uncharacteristic. They may only be attributed to a specific ion by correlation with the optical properties and by comparison of the resonance data with estimates from similar systems in diamagnetic hosts. Concerning the optical properties, TGG:Ce is a favourable case, because the bands of the host and impurity are spectrally resolved. The comparison with diamagnetic systems, on the other hand, is complicated by the presence of molecular fields. In summary, the exactness of EPR, not applicable in this regime, is replaced by rather crude information from ODMR.

It remains to be investigated whether the MCD-ODMR technique may also be applied for impurities in hosts showing magnetic ordering. In any case, a strong interaction with the Faraday rotation, common to such systems, should complicate corresponding experiments. This may lead to more severe problems than for TGG:Ce, since most of the impurity ions do not exhibit such a strong MCD signal as cerium does because of its strong spin–orbit coupling.

Acknowledgments

We thank Professor O F Schirmer for fruitful discussions and active help. The support of the Deutsche Forschungsgemeinschaft, SFB 225, is gratefully acknowledged.

Appendix A. Estimated resonance fields

The electronic configurations of Ce^{3+} and Tb^{3+} are $4f^1$ and $4f^8$, respectively, and the free-ion ground states are found to be $^2F_{5/2}$ and $^7F_6$. In the crystal field (CF) of symmetry D_2, corresponding to the local point symmetry of the rare-earth site in garnets, the $F_{5/2}$ state splits into three Kramers doublets, whereas the F_6 state splits into 13 singlets. The two lowest singlets are closely neighbouring in energy and may be regarded as a 'zero-field-split

† When writing elementary holograms, the spatial modulation of the light intensity results in a local modulation of the Ce^{3+} concentration by photochromism. Since the Ce^{3+} band contributes to the refractive index n, n is also modulated in space. This forms an elementary phase hologram. If such a hologram is written, the MCD will also be modulated in space. This may lead to interesting polarization-related effects during read-out depending on the applied magnetic field.

doublet' (*not* a Kramers doublet, of course). This two-singlet system of Tb and the lowest doublet from $F_{5/2}$ of Ce are schematically shown in the insets of figure 2. Only these states are occupied at low temperatures, and they determine the magnetic properties and the EPR transitions of both ions. We shall show now that the resonance fields $B_{\rm res}$ of the magnetic transitions for 36 and 70 GHz microwave frequency may be estimated using the effective-spin approach for the Ce doublet in connection with known X-band data (9 GHz), whereas a CF calculation within the F_6 multiplet may be used for the Tb ion. The interaction of the probe ion with the Tb-related bulk paramagnetism is neglected at first. Hence, the local effective magnetic field prevailing at the ion's site is meant whenever a magnetic field is mentioned in the following. The influence of molecular fields is discussed later.

A.1. Cerium

EPR data at X-band frequencies for Ce^{3+} in diamagnetic hosts are known for $Y_3Ga_5O_{12}$ [19] and $Y_3Al_5O_{12}$ [20]. Both analyses use the effective-spin approach with $S^{\rm eff} = 1/2$ and find the following effective g-values: $g_x^{\rm eff} = 2.738/2.00$, $g_y^{\rm eff} = 1.872/1.63$, and $g_z^{\rm eff} = 0.91/0.85$ for YAG and YGG, respectively. Here, the local x-axis is parallel to a cubic [100] axis, and the y- and z-axis are along [110] directions. Since the rare-earth site is similar in all garnets, one may expect that these g-values may serve as an estimate for $B_{\rm res}$ of Ce in TGG, too. However, we have to investigate whether the effective g-values obtained at X-band frequencies are also useful for 36 and 70 GHz. The latter is only true if the lowest doublet from $F_{5/2}$ of Ce is rather well decoupled from the excited $F_{5/2}$ levels. To examine this point we performed a simplified CF calculation using the parameters obtained in a study based on optical data for Ce^{3+} in YGG [21]. We converted the CF parameters $A_{kq}\langle r\rangle^k$ given in [21] to parameters B_{kq}, which are the coefficients of a CF expansion using Stevens operators O_{kq} [12]. The latter is a suitable approach if one confines the basis of states to the lowest multiplet of the free-ion case, i.e. to $F_{5/2}$ for Ce^{3+}. By numerical diagonalization of the matrix of the Hamiltonian

$$H = g_{\rm Landé}\boldsymbol{B}\cdot\boldsymbol{J} + \sum B_{kq}O_{kq}$$

within the states $F_{5/2}$, we found $g_{x,y,z}^{\rm eff} = 3.0, 1.5, 0.9$ and a distance of 150 cm^{-1} in zero field between the lowest and the next excited doublet. The latter was found to be 159 cm^{-1} in the analysis of reference [21], which includes $F_{7/2}$, and 139 cm^{-1} in the experiment [21]. Since our results agree sufficiently well with the literature, we may assume that the properties of the ground-state doublet are described reasonably well by our simple approach. The calculation shows that the effective g-values vary by less than 10^{-3} for transitions with 9, 36, and 70 GHz. It is now trivial to calculate $B_{\rm res}$ for Ce^{3+} at 36 and 70 GHz for $\boldsymbol{B} \parallel [111]$, the results being listed in table A1. For each entry two values are given, corresponding to the two magnetically inequivalent sites for the given orientation of $\boldsymbol{B}$. If we assume similar values for Ce in TGG and neglect the molecular fields (to be justified below), this result supports our assignment of the high-field ODMR signals to Ce ions. The resonances from the two inequivalent sites are not resolved in ODMR for 36 GHz due to the width of the signals, which is larger than the distance between the calculated values of $B_{\rm res}$. In the case of 70 GHz, possibly only the resonance of one site is within the range accessible with our magnet.

Table A1. Resonance fields in teslas of Ce^{3+} in YAG and YGG for 36 and 70 GHz ($\boldsymbol{B} \parallel [111]$), calculated according to data from references [19, 20].

Frequency	YGG	YAG
36	1.90, 1.46	1.46, 1.17
70	3.70, 2.82	2.84, 2.28

A.2. Terbium

No EPR data on Tb^{3+} ions in diamagnetic garnets are known, but reference [22] deals quantitatively with the properties of the two-singlet ground state of Tb^{3+} in TGG. In this paper, data on the electronic contribution to the specific heat and the magnetization are interpreted within the framework of a two-singlet model in combination with the molecular-field approximation. This model has been used before [23], mainly to attack the long-discussed problem of magnetic ordering for rare-earth compounds at zero temperature (see the first 14 references in [23]). A zero-field splitting $\Delta \approx 60$ GHz is found in [22] and, from the magnetization curves shown there, it should be possible to reach a conclusion on the Zeeman splitting of the two singlets and to estimate the magnetic resonance fields B_{res}. However, it is stated that the influence of the other excited states of the F_6 multiplet is not negligible and the calculation accounts for this influence by using a free parameter, for which no value is given. Hence, we cannot reach a conclusion on B_{res} from this calculation.

We therefore used the same approach as in the case of Ce^{3+}. The matrix of the Hamiltonian given above within the F_6 multiplet is diagonalized numerically, starting with the CF parameters of Tb^{3+} in YAG ([13], table 5, set (a)). As in the case of Ce, the parameters from [13] are converted for use with the operators O_{kq}. Our simplified approach yields similar energies for the seven lowest levels to the more elaborate calculation of reference [13], which includes all ^7F_J levels and the $^5D_4$ level. For example, $\Delta = 198$ GHz is found here, to be compared with $\Delta = 150$ GHz in [13]. The quality of such calculations may be estimated by comparing the results with the experimental value of $\Delta = 82.5$ GHz for YAG:Tb [13]. From this we conclude that the properties of the lowest singlets are well enough described in our approach and apply it as a starting point for TGG. The parameter set of YAG:Tb, even if modified over a wide range, leads to the result that the magnetic moment $\boldsymbol{m}$ of the two lowest singlets, induced by $\boldsymbol{B}$, is almost parallel to the local x-axis (see the preceding section) of each Tb ion. This may be expressed as $g_y^{\mathrm{eff}} \approx g_z^{\mathrm{eff}} \approx 0$. One may therefore apply the approximation $g_{y/z}^{\mathrm{eff}} = 0$, which simplifies the calculation of molecular fields considerably (see below). Its validity was postulated and supported by the results in [22–25]. For our task of finding estimates for B_{res}, $g_{y/z}^{\mathrm{eff}} = 0$ means that, for the experimental condition $\boldsymbol{B} \parallel [111]$, only one resonance field will be found instead of two, as required by symmetry. Our CF approach allows us to estimate quantitatively the error induced by this approximation. We find that the two resonance fields at 70 GHz differ by $\approx$70 mT, which is negligible with respect to the observed widths of resonances. One may further note that, as the two singlets have quenched momentum $\boldsymbol{J}$ at zero field, the magnetic moment per ion is determined by both the thermal occupation and the growth of $|\boldsymbol{J}|$ with increasing B. The magnetic properties of the lowest levels of Tb are therefore influenced by both paramagnetic and diamagnetic effects. This also affects the MCD.

For TGG we vary the nine B_{kq} under the constraint $\Delta = 60$ GHz to fit the curves

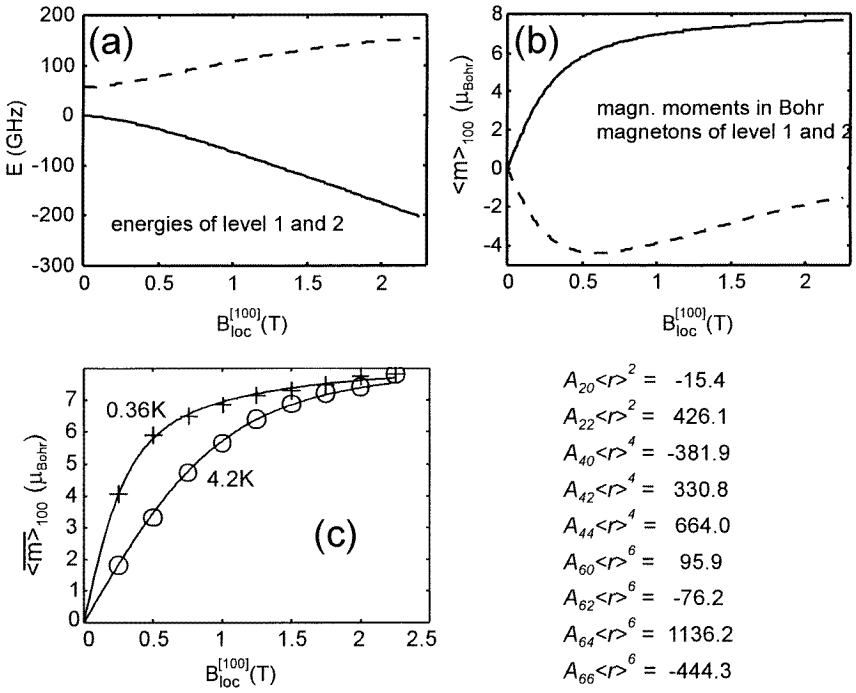

Figure A1. (a) The Zeeman diagram, (b) the expectation value of m_x for the two lowest levels of Tb^{3+}, and (c) the resulting thermal average of m_x at 0.36 and 4.2 K, in comparison with the experimental data from reference [22]. In each plot the abscissa refers to the [100] component of the local field (as in [22]). This is the relevant component under the assumption of complete anisotropy. The CF parameters used are given in the most widespread form as $A_{kq}\langle r\rangle^k$ in cm^{-1}.

$|\boldsymbol{m}|$ as functions of the *local* field $B_{\rm loc}$, given in [22] for 4.2 and 0.36 K†. The result is shown in figure A1, where also the Zeeman diagram and the expectation value of m_x for the two lowest levels is depicted. Such a fit is of course not unique since the number of parameters is too large in view of the experimental information, and the CF parameters listed in the figure (as $A_{kq}\langle r\rangle^k$) are given as representative values only. However, since the magnetization curve is well described, at least the Zeeman splitting of the two-singlet ground state should be suited for estimating $B_{\rm res}$ for Tb in TGG. Neglecting the molecular fields (see below), the resonance field for 70 GHz is found to be $\approx$0.35 T, approximately valid for both magnetically inequivalent centres, as stated above. The value appears to be too small in view of the ODMR resonance field for 70 GHz of $\approx$0.7 T. We conclude that a value of slightly less than 60 GHz applies for Δ of Tb^{3+} in TGG.

It should be noted that $B_{\rm res}$ strongly depends on the crystal field, since the transition occurs in the vicinity of the zero-field splitting, where the Zeeman levels still depend only weakly on the magnetic field (see figure A1). Crystal inhomogeneities, leading to a distribution of CF parameters, or phonon modulation of the crystal field will therefore provide an efficient mechanism for the broadening of the resonance lines, as is usual for

† A similar procedure has been applied to interpret high-field magnetization experiments in [26]. We did not use the CF parameters given there, since Lorentz fields are not considered and the result $\Delta = 84$ GHz is in conflict with our ODMR results.

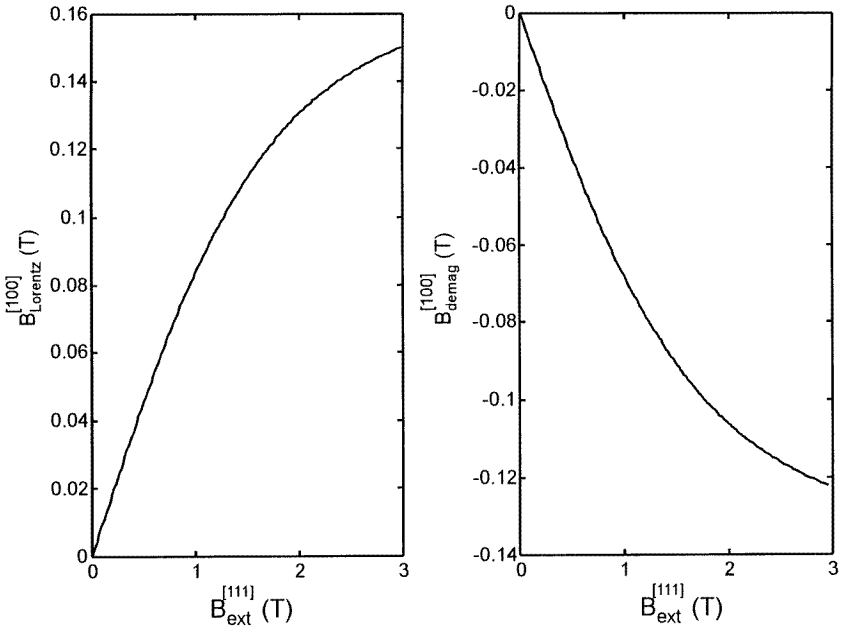

Figure A2. The x-component of the molecular fields B_{Lorentz} and B_{demag} as a function of the external magnetic field along [111]. Only this component is relevant for a single ion from the sublattices α, α' in the approximation of complete anisotropy (see the text).

non-Kramers ions. The latter is a concrete example for the fluctuating, line-broadening fields mentioned in [4]. Since the Ce ions are exposed to the dipolar magnetic field of the terbium neighbours, both the static and the dynamic fluctuations of the magnetic moments of Tb^{3+} will lead to a broadening of the Ce-related magnetic resonances, too.

A.3. The influence of molecular fields

We shall now justify the neglect of the molecular fields in the preceding sections. In the case of purely dipolar interaction, assumed to be valid here [22], the usual superposition scheme for the local field may be applied:

$$\boldsymbol{B}_{\mathrm{loc}} = \boldsymbol{B}_{\mathrm{ext}} + \boldsymbol{B}_{\mathrm{Lorentz}} + \boldsymbol{B}_{\mathrm{demag}}. \tag{A1}$$

Here, $\boldsymbol{B}_{\mathrm{Lorentz}}$ comprises the sum of the fields of the dipoles within the Lorentz sphere and the uncompensated dipoles on the surface of the sphere, and $\boldsymbol{B}_{\mathrm{demag}}$ is the demagnetization field.

The lattice sums, necessary to estimate $\boldsymbol{B}_{\mathrm{Lorentz}}$, have been computed for the two-singlet case in garnets under the assumption of complete anisotropy ($g^{\mathrm{eff}}_{y/z} = 0$) in references [24, 25]. Under this assumption and in the paramagnetic regime, the dipolar field set up by the ions with the local x-axis x_{loc} parallel to [100] (sublattice α, α' in [24], where our x_{loc} is named z) does not act on the other two groups of ions, having $x_{\mathrm{loc}} \parallel [010]$ or $\parallel [001]$ (sublattices β, β' and γ, γ' in references [24, 25]). This follows from site symmetry. In other words, the ions belonging to the sublattices α, α', β, β', and γ, γ' are mutually decoupled [24]. These three sublattices are equivalently magnetized for $\boldsymbol{B} \parallel [111]$. Therefore we are free to choose a Tb ion from the sublattice α, α' as the probe ion. For

this case, the expression for $\boldsymbol{B}_{\text{Lorentz}}$, which is $\parallel$ [100] for α, α', may be taken from the last row of table I of reference [25]. This row refers to a parallel dipole alignment, which is appropriate to the paramagnetic case (independent dipoles, parallel in thermal average). With the lattice constant of 12.36 Å for TGG [1], the numerical value for the molecular-field constant is found to be 21 mT/μ_{Bohr}, so $B^{[100]}_{\text{Lorentz}} = 0.021\langle\bar{m}\rangle$, where $\langle\bar{m}\rangle$ is the thermally averaged magnetic moment of a single ion in multiples of μ_{Bohr} (see figure A1).

The usual approximation for the demagnetization field, $\boldsymbol{B}_{\text{demag}} = -N\mu_0\boldsymbol{M}$, is used, where N is the demagnetization factor and $\boldsymbol{M} = \langle\bar{m}\rangle\rho(1,1,1)/\sqrt{3}$ is the macroscopic magnetization, with the ion density ρ. As N is not strictly defined for cylindrically shaped probes, we take N for an ellipsoid of revolution (see, e.g., reference [27]) of similar size to our samples.

Since both $\boldsymbol{B}_{\text{Lorentz}}$ and $\boldsymbol{B}_{\text{demag}}$ depend on $\langle\bar{m}\rangle$, which is a function of the local field, the molecular-field equation (A1) must be evaluated self-consistently, which is trivial with a numerical computer program. The values for $\langle\bar{m}\rangle = f(B_{\text{local}})$ are obtained as described in the preceding section. Figure A2 shows, as a function of the external magnetic field along [111], the [100] component of $\boldsymbol{B}_{\text{Lorentz}}$ and $\boldsymbol{B}_{\text{demag}}$ for a probe with the dimensions of S1, which is the sample mainly discussed here. Only the [100] component is relevant to our probe ion taken from sublattice α, α'. Obviously, the two fields nearly cancel and the small residual value may be neglected considering the crudeness of our estimates. The cancellation of the molecular fields is of course accidental, as it depends on the shape of the samples. We checked the effect of B_{demag} on the 70 GHz ODMR line of Tb by comparing the positions of this line for samples S3a (a flat disc) and S3b (a cylinder). The line positions were $\approx$0.7 T for S3b (as for S1; see figure 2, spectrum C) and $\approx$0.95 T for S3a (figure 4). These positions collapse at 0.5 ± 0.05 T, when the contributions of the—different—fields B_{demag} are subtracted in both cases.

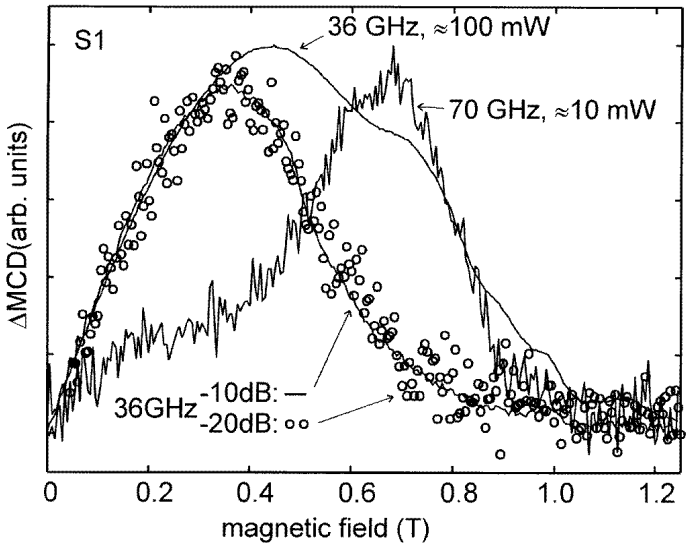

Figure A3. ODMR spectra at 36 GHz with ≈100 mW and with reduced power. The shoulder on the right-hand side of the high-power spectrum is attributed to two-quanta transitions occurring at approximately the same position as the ODMR observed using 70 GHz.

Appendix B. Peculiar features of the ODMR spectra

We shall now try to explain the unusual features of the ODMR spectra in figure 2. This is important, because these spectra are very distinct from the results obtained from isolated paramagnetic ions in diamagnetic hosts. In order to give a firm attribution of the ODMR to certain ions, as many experimental details as possible should be understood.

(i) An ODMR band assigned to Tb^{3+} at low magnetic fields is observed for 36 GHz, although the zero-field splitting of the lowest two Tb levels is of the order of 60 GHz, or slightly less. This feature is easily explained by assuming a distribution or a modulation of the CF parameters, which, as mentioned in the previous section, is responsible for the ODMR line broadening. For simplicity one may think of a distribution of Δ, the zero-field splitting of the two lowest singlets of Tb^{3+}. From spectrum C in figure 2 we find a full width at half-maximum for the Tb ODMR of $\approx$0.4 T. According to the Zeeman diagram shown in figure A1, this width corresponds to a width of $\pm$30 GHz for the distribution of Δ. Consequently, microwave quanta of 36 GHz may induce transitions at low magnetic fields starting from zero. As the shape of the ODMR signal depends on the form of the distribution of Δ, it is accidental that the maximum of the ODMR at 36 GHz is approximately at half the field observed for 70 GHz. The situation at 36 GHz is further complicated by two-quanta transitions at higher microwave power. For this reason the ODMR spectrum A in figure 2 was recorded with the power reduced by 10 dB. In figure A3 this resonance is shown again, with an ODMR spectrum recorded with 20 dB attenuation superposed on it. The latter has been scaled to the same height to verify a constant shape. For maximum power impinging on the sample ($\approx$100 mW), a shoulder grows up at higher fields. This shoulder is attributed to two-quanta transitions, as it quickly disappears when the power is reduced. This is a typical behaviour of such transitions. In addition, the shoulder appears at a field where the ODMR for 72 GHz is expected. To illustrate this we added an ODMR spectrum for 70 GHz to the figure.

(ii) The Tb ODMR is also seen when the Ce MCD serves as a monitor (curves B and D, 416 nm). This is surprising at first glance, since the resonances of paramagnetic ions are usually detected nicely separated via the respective MCD bands, if these bands do not overlap, as is the case here. Obviously, the resonance transitions of the Tb ions affect the MCD of Ce, and some coupling between the spin systems must therefore be taken into account. Cerium and terbium ions are rather close in TGG, the nearest distance of ions at regular rare-earth sites being $\approx$3.8 Å (calculated from structural data [1]). Using the results of the preceding section, one may estimate about 90 mT for the dipolar field which a single Tb ion exerts at a nearest-neighbour Ce site (assumed to be substitutional for Tb). There exists therefore an important spin–spin interaction, even if exchange between Ce and Tb is neglected. The latter is known to be a good approximation for the interaction among the Tb ions alone in TGG [22]. Since the spin systems of Ce and Tb are thus coupled effectively, it is reasonable that any microwave-induced change of the thermal occupation of the spin states (or, more appropriately, the total angular momentum states) of Tb may affect the spin temperature of Ce, too. In this way ODMR transitions of Tb can be detected via the MCD of the cerium impurities. The effect of magnetic resonance transitions of Ce on the MCD of the bulk ions Tb, on the other hand, is obviously too small to be detectable.

(iii) When monitoring the MCD of Ce, there is additional signal intensity at 0.9 T on the shoulder of the Tb ODMR band leading to an apparent shift of this band (see curves D and B of figure 2). Our estimates for the expected resonance positions of Ce^{3+} (appendix A) show that it is unlikely that this shift is due to an additional Ce resonance. Rather it is

an effect of bulk, i.e. terbium-related, magnetic transitions. We have argued above that the detection of these transitions via the MCD of Ce may be conceived as a transfer of heat from the bulk dipolar system to the spins of the impurities. For simplicity let us postulate equal spin temperatures for the two systems. For a given rate of transition between the lowest Tb levels a certain rise in spin temperature δT_S will result. In other words, the occupation difference ΔP of the lowest (quasi-) doublets will decrease under the influence of the microwave heating. For the same δT_S, ΔP is larger for Ce than for Tb, since the splitting of the magnetic levels ΔE at a given field is much smaller for Ce than for Tb (see the insets of figure 2 or appendix A). Moreover, ΔP, related to a certain δT_S, drops much more quickly towards zero for Tb than for Ce, because ΔE increases steeply for Tb, as compared to Ce. Since the MCD is proportional to ΔP, the ODMR signal of Tb may be detected up to higher fields using the Ce MCD instead of the MCD of Tb itself.

(iv) In the region between 1.3 and 2.5 T (figure 2, curve D, 70 GHz) and above 2 T (curve B, 36 GHz) a flat 'background' signal is observed, which is much weaker when Tb is the monitor ion. For Tb this background only appears when using the stronger microwave source at 36 GHz (figure 2, trace A). We assume that these signals arise from non-resonant heating of the spin systems via the interaction of the microwave field with the bulk magnetization. For the same reasons as discussed above, the rise in temperature is more efficiently observed via the MCD of Ce than that of Tb. We also attribute the flat ODMR signal below ≈ 0.3 T to this non-resonant heating effect. This non-resonant absorption is responsible for a substantial detuning of the microwave bridge if a TGG sample is placed in a conventional EPR spectrometer. Absorption of a microwave field by the (macroscopic) magnetization is described by an imaginary part χ'' of the complex susceptibility. In a microscopic view, χ'' is related to transitions between the levels that carry the magnetic moments. In our case these levels are those of Tb^{3+}. Non-resonant absorption may be conceived as simultaneous up–down transitions of a number of Tb ions. Such multi-centre transitions are favoured by the relatively strong interaction between the magnetic moments of Tb. The net energy of a multi-centre transition must correspond to the energy of a microwave quantum. This condition may be fulfilled in a non-resonant way, since the energy distances between the Tb levels are distributed in a broad band around a resonance value (leading to the observed broadness of the ODMR bands).

References

[1] *Landolt–Börnstein New Series* 1970 Group III, vol 4b, ed K-H Hellwege (Heidelberg: Springer) p 1ff
Landolt–Börnstein New Series 1978 Group III, vol 12a, ed K-H Hellwege (Heidelberg: Springer) p 265ff
Landolt–Börnstein New Series 1991 Group III, vol 27e, ed K-H Hellwege (Heidelberg: Springer) p 136ff

[2] Sugg B, Nürge H, Faust B, Ruža E, Niehüser R, Reyher H-J, Rupp R A and Ackermann L 1995 *Opt. Mater.* **4** 343

[3] Agulló-López F (ed) 1995 *Insulating Materials for Optoelectronics* (Singapore: World Scientific)

[4] Hutchings M T and Wolf W P 1963 *Phys. Rev. Lett.* **11** 187

[5] Hutchings M T, Windsor C G and Wolf W P 1966 *Phys. Rev.* **148** 444

[6] Göbbels M 1992 *PhD Thesis* RWT, Aachen

[7] Pogatshnik G J, Chain L S, Chen Y and Evans B D 1991 *Phys. Rev.* **43** 1787

[8] Spaeth J-M and Lohse F 1990 *J. Phys. Chem. Solids* **51** 861

[9] Henderson B and Imbusch G F 1989 *Optical Spectroscopy of Inorganic Solids* (Oxford: Clarendon)

[10] Reyher H-J, Schulz R and Thiemann O 1994 *Phys. Rev.* B **50** 3609

[11] Jensen H P, Schellman J A and Troxell T 1978 *Appl. Spectrosc.* **32** 192

[12] Hüfner S 1978 *Optical Spectra of Transparent Rare Earth Compounds* (New York: Academic)

[13] Bayerer R, Heber J and Mateika D 1986 *Z. Phys.* B **64** 201

[14] Jacobs R R, Krupke W F and Weber M J 1978 *Appl. Phys. Lett.* **33** 410

[15] Hamilton D S, Gayen S K, Pogatshnik G J, Ghen R D and Miniscalco W J 1989 *Phys. Rev.* B **39** 8807

[16] Buckingham A D and Stephens P J 1966 *Annu. Rev. Phys. Chem.* **17** 399
[17] Denning R G 1975 The technique of magnetic circular dichroism *Electronic States of Inorganic Compounds: New Experimental Techniques* ed P Day (Boston: Reidel) p 157
[18] Weber M J 1973 *Solid State Commun.* **12** 741
[19] White R L, Phillips T G and Lefever R A 1967 *J. Appl. Phys.* **38** 408
[20] Lewis H R 1966 *J. Appl. Phys.* **37** 739
[21] Herrmann G F, Pearson J J, Wickersheim K A and Buchanan R A 1966 *J. Appl. Phys.* **37** 1312
[22] Hammann J and Manneville P 1973 *J. Physique* **34** 615
[23] Bidaux R, Gavignet-Tillard A and Hammann J 1973 *J. Physique* **34** 19
[24] Bidaux R and Vivet B 1968 *J. Physique* **29** 57
[25] Gavignet-Tillard A, Hammann J and De Seze L 1973 *J. Physique* **34** 27
[26] Guillot M, Marchand A, Nekvasil V and Tcheou F 1985 *J. Phys. C: Solid State Phys.* **18** 3547
[27] Morrish A H 1980 *The Physical Principles of Magnetism* (New York: Krieger)